Allowed and forbidden transitions in an atom placed near an ideally conducting cylinder

V. V. Klimov*

P. N. Lebedev Physical Institute, Russian Academy of Sciences, 53 Lenin Prospect, Moscow 117924, Russia

M. Ducloy

*Laboratoire de Physique des Lasers, UMR CNRS 7538, Institute Galilée, Université Paris-Nord, Avenue J-B. Clément,
F 93430 Villetaneuse, France*

The properties of dipole-allowed and -forbidden (quadrupole) transitions in an atom placed near an ideally conducting cylinder are considered. Explicit analytical expressions for transition rates for different orientations of dipole and quadrupole are found. It is shown that the decay rates of dipole and quadrupole transitions with radially oriented moments tend to infinity when the cylinder radius tends to zero. On the other hand, for tangential orientation (φ orientation), the dipole transition rate decreases while the quadrupole transition rate increases substantially. As a result, the quadrupole decay rates may approach the dipole decay rates. Such behavior has analogy in neither spherical nor plane geometry of the metal interface.

I. INTRODUCTION

It is well known that the rates of quadrupole transitions in the optical region are lower by a factor of $(a_0/\lambda)^2 \propto 10^{-6}-10^{-8}$ (where a_0 is the Bohr radius and λ is the radiation wavelength) than those of their dipole counterparts [1] and that the dipole transition probability is strongly influenced by the presence of macroscopic bodies near the radiating atom (see, for example, [2,3]. The question arises in this connection: How do material bodies affect quadrupole or multipole transitions?

To explain this problem let us consider the amplitude of the decay of an excited atomic state to a lower-energy state, accompanied by the emission of a photon. In that case, the transition matrix element has the form

$$V \propto \int \psi_{\text{out}}^*(\mathbf{r}) \boldsymbol{\nabla} \cdot [\psi_{\text{in}}(\mathbf{r}) \mathbf{A}(\mathbf{r})] d\mathbf{r},$$

where $\mathbf{A}$ is the wave function of the photon emitted, with allowance made for the presence of material bodies, and ψ_{in} (ψ_{out}) is the wave function of the excited (unexcited) state. As in the case of free space, the wave functions of the atom $\psi(\mathbf{r})$ vary faster than the wave function of the photon, and this allows one to expand the wave function of the photon into a series in powers of coordinates in the vicinity of the atom. Where dipole radiation is forbidden, the first term in this series goes to zero, and the value of the matrix element is governed by that of the gradient of the photon wave function in the neighborhood of the atom, which is supposed to be at $\mathbf{r}_0$:

$$V \propto \frac{\partial}{\partial r_{0,j}} A_i(\mathbf{r}_0) \int \psi_{\text{out}}^*(\mathbf{r}) \frac{\partial}{\partial r_i} \psi_{\text{in}}(\mathbf{r}) r_j d\mathbf{r}.$$

A principal difference between the case in hand and that of free space is that the scale of the gradient of the photon wave function depends, generally speaking, not only on the radiation wavelength, but also on the characteristic size of the problem. Moreover, in the case of an atom located close to a material body with a small radius of curvature a, the wave-function gradient is determined mainly by the surface curvature of the body and not by the radiation wavelength in free space. As a result, the quadrupole radiation probability increases faster as compared with that in the case of free space. Note the fact that, when the characteristic geometrical size of the problem is close to the size of the atomic orbit, the radiation intensity may approach the intensity of dipole transitions. Specifically, for Rydberg and closely similar atoms, the orbit size may be as great as 10^{-5} cm, and so one can create appropriate geometrical conditions for observation of the enhancement of quadrupole transitions.

The increasing of quadrupole transition rates near the surface of a dielectric microsphere was demonstrated in [4,5]. However, geometries different from the dielectric microsphere are being investigated actively now. Recently, the cavity QED effects near a solid dielectric cylinder have also become interesting and attractive, in particular, in the fields of atom optics and atomic spectroscopy in a microcavity. For instance, it has been suggested that stable helical motion of an atom around a solid optical fiber may be possible by using evanescent waves developed near the cylindrical surface [6]. Moreover, a quantum nondemolition measurement of the photon number inside an optical fiber has been performed using Compton scattering of the electrons due to evanescent waves produced near the fiber [7]. The falling of atoms on the singular potential of a charged metal wire was demonstrated in an experiment [8]. In [9], use of dielectric fiber was suggested to detect nondiagonal terms in the van der Waals force.

In this paper, we investigate the influence of ideally conducting cylindrical surface on rates of allowed (dipole) and forbidden (quadrupole) transitions. The geometry of the problem under investigation is shown in Fig. 1. According to

_____
*Email address: klimov@rim.phys.msu.su
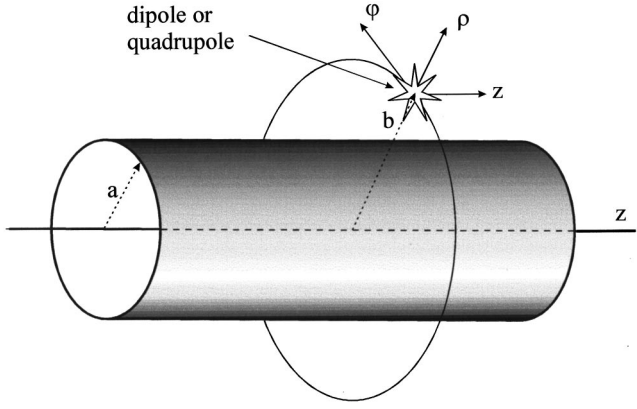
FIG. 1. Geometry of the problem.

[2,3], classical and quantum-electrodynamical calculations give the same result for the dipole transition rate normalized to its vacuum value. In [4] for the example of a dielectric microsphere the same connection between classical and calculations of quadrupole rates was shown. In the present paper we shall investigate the influence of an ideally conducting cylinder on transition rates within the classical as well as the QED approach and show their equivalence.

In general, the problem of radiation from a point source near an ideally conducting cylindrical surface is classical and well investigated [10–12]. The transition rates of a dipole inside an ideally conducting cylinder were found in [13]. In [14] some plots of dipole rates in an atom near a cylinder were presented. Nevertheless, a detailed analysis of allowed and forbidden transitions near a cylinder has not been carried out as far as we know. The results obtained reveal a substantial increase of dipole and quadrupole rates in comparison with the case of spherical or plane geometry.

The plan for the rest of the work is as follows. In Sec. II the influence of a cylinder on dipole transition rates is investigated and explicit analytical expressions are obtained for any dipole orientation. In Sec. III the influence of a cylinder on quadrupole transition rates is investigated and explicit analytical expressions are obtained for any quadrupole orientation. Section IV is devoted to analysis of the expressions for rates obtained in Secs. II and III. In this section also the results obtained are compared with those for spherical and plane geometries. In the Conclusion we sum up and outline the directions of further investigation. In the Appendix we present the QED derivation of decay rates for any dipole or quadrupole transition in an atom placed near an ideally conducting cylinder.

II. DIPOLE (ALLOWED) TRANSITIONS NEAR AN IDEALLY CONDUCTING CYLINDER

Let us consider a classical oscillator located at the point $\mathbf{r}'$ near an ideally conducting cylinder as a model of an atom. We suppose that the oscillator and cylinder are in vacuum. The geometry of the problem is presented in Fig. 1. In the classical approach, the change in the radiation linewidth is associated with the radiation backreaction. If the atom is treated as a nonrelativistic oscillator consisting of a station-

ary charge $-e$ and a charge e oscillating about it, the equation of motion of the latter in vacuum has the form

$$m\,\delta\ddot{\mathbf{r}} = \frac{2e^2}{3c^3}\,\delta\dddot{\mathbf{r}} - m\omega_0^2\,\delta\mathbf{r}, \qquad (1)$$

or, in the case of weak radiation reaction,

$$m\,\delta\ddot{\mathbf{r}} + m\,\gamma_{\mathrm{dip},0}\delta\dot{\mathbf{r}} + m\omega_0^2\,\delta\mathbf{r} = \mathbf{0},$$

$$\gamma_{\mathrm{dip},0} = \frac{2e^2}{3c^3}\frac{\omega_0^2}{m}. \qquad (2)$$

Here $\gamma_{0,\mathrm{dip}}$. is the spontaneous linewidth in vacuum, $\delta\mathbf{r}$ is the displacement of the moving charge from the balanced state, and ω_0 is the frequency of oscillations in vacuum. If the oscillator is located at the point $\mathbf{r}'$ near a cylinder, it is acted upon by an additional (compared to the case of free space) field $\mathbf{E}^{(1)}(\mathbf{r}')$, so that its equation of motion assumes the form

$$m\,\delta\ddot{\mathbf{r}} + m\,\gamma_{\mathrm{dip},0}\delta\dot{\mathbf{r}} + m\omega_0^2\,\delta\mathbf{r} = e\mathbf{E}^{(1)}(\mathbf{r}' + \delta\mathbf{r},t) \approx e\mathbf{E}^{(1)}(\mathbf{r}',t),$$

$$m\ddot{\mathbf{d}} + m\,\gamma_{\mathrm{dip},0}\dot{\mathbf{d}} + m\omega_0^2\mathbf{d} = e^2\mathbf{E}^{(1)}(\mathbf{r}',t), \qquad (3)$$

where $\mathbf{d} = e\,\delta\mathbf{r}$ is the electric dipole moment of the atomic transition. To find the reflected field it is necessary to solve the full system of Maxwell's equations in which the source is the dipole oscillator moment.

Projecting Eq. (3) onto the oscillation direction, we get

$$m\ddot{d} + m\,\gamma_{\mathrm{dip},0}\dot{d} + m\omega_0^2 d = e^2\frac{\mathbf{d}_0 \cdot \mathbf{E}^{(1)}(\mathbf{r}',t)}{d_0}, \qquad (4)$$

where d_0 is the dipole oscillation amplitude. Assuming that all the quantities involved are proportional to $\exp(-i\omega t)$ from Eq. (4), we obtain the following dispersion equation to define the line characteristics in the presence of any body:

$$\omega^2 + i\omega\gamma_{\mathrm{dip},0} - \omega_0^2 + \frac{e^2}{md_0^2}\mathbf{d}_0 \cdot \mathbf{E}^{(1)}(\mathbf{r}',\omega) = 0. \qquad (5)$$

In the following we will assume that a perturbation approach can be applied. Then the solution of Eq. (5) may be written in the form

$$\omega = \omega_0 - \frac{i}{2}\,\gamma_{\mathrm{dip},0} - \frac{e^2}{2m\omega_0}\frac{\mathbf{d}_0 \cdot \mathbf{E}^{(1)}(\mathbf{r}',\omega_0)}{d_0^2}. \qquad (6)$$

Separating real and imaginary parts of this expression and using expression (2) for the linewidth in vacuum, we obtain in this approximation the formula for the linewidth change (see, for example, [2]),

$$\frac{\gamma_{\mathrm{dip}}}{\gamma_{\mathrm{dip},0}} = 1 + \frac{3}{2}\,\mathrm{Im}\frac{\mathbf{d}_0 \cdot \mathbf{E}^{(1)}(\mathbf{r}',\omega_0)}{d_0^2 k^3}. \qquad (7)$$

Hereafter, $k = \omega/c \approx \omega_0/c$ stands for the wave vector in free space.

Thus the reflected field must be found to determine the radiative linewidth (transition rate, decay rate). To find the reflected field, it is necessary to solve the full system of Maxwell's equations where the dipole moment of the oscillator is the source. This solution is well known in the case of an ideally conducting cylinder [10–12].

For our purpose the approach of Ref. [10] is most convenient. According to this approach, the longitudinal components of the electric and magnetic fields are expressed through the densities of external charges and currents,

$$E_z(\mathbf{r}) = \int d\mathbf{r}' \left(ik \frac{j_z(\mathbf{r}')}{c} + \rho(\mathbf{r}') \frac{\partial}{\partial z'} \right) G_1(\mathbf{r}, \mathbf{r}'), \quad (8)$$

$$H_z(\mathbf{r}) = \frac{1}{c} \int d\mathbf{r}' [\mathbf{j}(\mathbf{r}') \times \mathbf{\nabla}']_z G_2(\mathbf{r}, \mathbf{r}'). \quad (9)$$

In Eqs. (8) and (9) G_1 and G_2 stand for Green's functions satisfying boundary conditions of the first and second types on the cylinder surface:

$$G_1(\mathbf{r}, \mathbf{r}') = \frac{i}{2} \sum_{n=-\infty}^{n=\infty} \int dh \, e^{ih(z-z') + in(\varphi - \varphi')} H_n^{(1)}(\nu\rho)$$

$$\times \left(J_n(\nu\rho') - H_n^{(1)}(\nu\rho') \frac{J_n(\nu a)}{H_n^{(1)}(\nu a)} \right), \quad (10)$$

$$G_2(\mathbf{r}, \mathbf{r}') = \frac{i}{2} \sum_{n=-\infty}^{n=\infty} \int dh \, e^{ih(z-z') + in(\varphi - \varphi')} H_n^{(1)}(\nu\rho)$$

$$\times \left(J_n(\nu\rho') - H_n^{(1)}(\nu\rho') \right.$$

$$\left. \times \frac{(d/dz)[J_n(z)]}{(d/dz)[H_n^{(1)}(z)]} \right|_{Z=\nu a} \right). \quad (11)$$

Here we use the cylindrical frame of reference $\mathbf{r} = (\rho, \varphi, z)$ and put the observation point $\mathbf{r}$ at $\rho > \rho'$, where ρ' is the radial coordinate of the oscillator. In Eqs. (10) and (11) h is the wave number along the z axis and $\nu = \sqrt{k^2 - h^2}$ is the radial wave number. The integration contour over h in Eqs. (10) and (11) lies on the real axis if the wave vector k has infinitely small imaginary part ($k \rightarrow k + i\varepsilon$). Note that in Eqs. (10) and (11) the first terms [containing the factor $J_n(\nu\rho')$] are related to the free-space Green's function while the second terms [containing the factor $H_n^{(1)}(\nu\rho')$] are related to reflected fields.

The remaining field components can be expressed through the z component of either the electric (TM modes) or the magnetic field (TE modes):

$$E_{\rho,h}^{\mathrm{TM}} = \frac{ih}{\nu^2} \frac{\partial E_{z,h}}{\partial \rho}, \quad E_{\varphi,h}^{\mathrm{TM}} = \frac{ih}{\nu^2} \frac{\partial E_{z,h}}{\rho \partial \varphi}, \quad (12)$$

$$E_{\rho,h}^{\mathrm{TE}} = \frac{ik}{\nu^2} \frac{\partial H_{z,h}}{\rho \partial \varphi}, \quad E_{\varphi,h}^{\mathrm{TE}} = -\frac{ik}{\nu^2} \frac{\partial H_{z,h}}{\partial \rho}. \quad (13)$$

In Eqs. (12) and (13) the subscript h denotes the appropriate Fourier transformation over z. The full field is defined by the sum of the TM and TE components.

Expressions for the charge density and the current of a dipole oscillator placed at $\mathbf{r}'$ can be produced in the regular form

$$\rho = -(\mathbf{d}_0 \cdot \mathbf{\nabla}) \delta(\mathbf{r} - \mathbf{r}') e^{-i\omega t},$$

$$\mathbf{j} = -i\omega \mathbf{d}_0 \delta(\mathbf{r} - \mathbf{r}') e^{-i\omega t}, \quad (14)$$

complying with the law of charge conservation. Here δ is Dirac's delta function. Substituting these expressions into Eqs. (8) and (9) and integrating by parts one can find the components of the electric field that we need. As a result of using Eq. (7), the final expression for the relative rate of dipole transitions of an atom placed at $\mathbf{r}' = (\rho' = b, \varphi' = 0, z' = 0)$ near a metal cylinder takes the following form:

$$\frac{\gamma_{\mathrm{dip}}}{\gamma_{\mathrm{dip},0}} = 1 - \tfrac{3}{2} \operatorname{Re}(W). \quad (15)$$

In the case of ρ and φ orientations of the dipole, both TM and TE modes give contributions to the decay rate:

$$W_\rho = \sum_{n=-\infty}^{\infty} \int_0^k dh \frac{h^2}{k^3} \left(\frac{d}{dz}[H_n^{(1)}(z)] \Big|_{z=\nu b} \right)^2 \frac{J_n(\nu a)}{H_n^{(1)}(\nu a)}$$

$$+ \sum_{n=-\infty}^{\infty} \int_0^k dh \frac{n^2}{k} \left(\frac{H_n^{(1)}(\nu b)}{\nu b} \right)^2 \frac{(d/dz)[J_n(z)]|_{z=\nu a}}{(d/dz)[H_n^{(1)}(z)]|_{z=\nu a}}, \quad (16)$$

$$W_\varphi = \sum_{n=-\infty}^{\infty} \int_0^k dh \frac{h^2 n^2}{k^3 (\nu b)^2} \frac{[H_n^{(1)}(\nu b)]^2 J_n(\nu a)}{H_n^{(1)}(\nu a)}$$

$$+ \sum_{n=-\infty}^{\infty} \int_0^k \frac{dh}{k}$$

$$\times \frac{\{(d/dz)[H_n^{(1)}(z)]|_{z=\nu b}\}^2 (d/dz)[J_n(z)]|_{z=\nu a}}{(d/dz)[H_n^{(1)}(z)]|_{z=\nu a}}. \quad (17)$$

In the case of z orientation of the dipole only TM modes give contributions to the decay rate:

$$W_z = \sum_{n=-\infty}^{\infty} \int_0^k dh \frac{\nu^2}{k^3} \frac{[H_n^{(1)}(\nu b)]^2 J_n(\nu a)}{H_n^{(1)}(\nu a)}. \quad (18)$$

In all of these cases $\nu = \sqrt{k^2 - h^2}$ is the radial wave number.

It is interesting that in Eqs. (16)–(18) integration over the wave number h is restricted by k. This is due to the fact that at $h > k$ there are no propagating waves that can carry off energy to infinity.

The expressions (15)–(18) have a form that is useful for some analytical investigations. However, it is difficult to recognize from Eqs. (15)–(18) that decay rates are positive quantities. If one calculates decay rates within the quantum

approach through Fermi's golden rule, it is possible to obtain instead of Eqs. (15)–(18) the explicitly positive expressions (for details see the Appendix)

$$
\frac{\gamma_{\mathrm{dip},\rho}}{\gamma_{\mathrm{dip},0}} = \frac{3}{2} \sum_{n=-\infty}^{\infty} \int_0^k dh \frac{h^2}{k^3} \left[\frac{d}{dz}[J_n(z)] \right|_{z=\nu b}
$$
$$
- \frac{J_n(\nu a)}{H_n^{(1)}(\nu a)} \frac{d}{dz}[H_n^{(1)}(z)] \bigg|_{z=\nu b} \right]^2
$$
$$
+ \frac{3}{2} \sum_{n=-\infty}^{\infty} \int_0^k dh \frac{n^2}{k(\nu b)^2} \left[J_n(\nu b) \right.
$$
$$
- \frac{(d/dz)[J_n(z)]|_{z=\nu a}}{(d/dz)[H_n^{(1)}(z)]|_{z=\nu a}} H_n^{(1)}(\nu b) \right]^2, \quad (19)
$$

$$
\frac{\gamma_{\mathrm{dip},\varphi}}{\gamma_{\mathrm{dip},0}} = \frac{3}{2} \sum_{n=-\infty}^{\infty} \int_0^k dh \frac{h^2 n^2}{k(kb)^2 \nu^2} \left[J_n(\nu b) - \frac{J_n(\nu a)}{H_n^{(1)}(\nu a)} \right.
$$
$$
\times H_n^{(1)}(\nu b) \right]^2 + \frac{3}{2} \sum_{n=-\infty}^{\infty} \int_0^k \frac{dh}{k} \left[\frac{d}{dz}[J_n(z)] \right|_{z-\nu b}
$$
$$
- \frac{(d/dz[J_n(z)]|_{z=\nu a}}{(d/dz)[H_n^{(1)}(z)]|_{z=\nu a}} \frac{d}{dz}[H_n^{(1)}(z)] \bigg|_{z=\nu b} \right]^2,
$$
$$
\qquad (20)
$$

$$
\frac{\gamma_{\mathrm{dip},z}}{\gamma_{\mathrm{dip},0}} = \frac{3}{2} \sum_{n=-\infty}^{\infty} \int_0^k dh \frac{\nu^2}{k^3} \left[J_n(\nu b) - \frac{J_n(\nu a)}{H_n^{(1)}(\nu a)} H_n^{(1)}(\nu b) \right]^2.
$$
$$
\qquad (21)
$$

Using the identities

$$
\sum_{n=-\infty}^{n=\infty} J_n^2(z) = 1, \quad \sum_{n=-\infty}^{n=\infty} n^2 J_n^2(z) = \frac{z^2}{2},
$$

$$
\sum_{n=-\infty}^{n=\infty} \left(\frac{dJ_n(z)}{dz} \right)^2 = \frac{1}{2},
$$

one can show the equivalence of Eqs. (15)–(18) and (19)–(21), i.e., the equivalence of the classical and quantum approaches.

From Eqs. (15)–(18) it is easy to see that when an atom has moved to infinity ($b \to \infty$) the reflected field tends to zero and the radiative linewidth tends to unity. The behavior of these rates becomes more interesting as an atom approaches the cylinder surface ($b \to a$). In this case one can see from Eqs. (20) and (21) that the transition rates for tangential orientations (φ, z) of the dipole vanish independently of the radius of cylinder. On the other hand, the decay rate of a radially oriented dipole located on the surface ($a = b$) does not vanish:

$$
\left(\frac{\gamma}{\gamma_0} \right)_{\mathrm{dip},\rho} = \frac{6}{\pi^2} \sum_{n=-\infty}^{\infty} \int_0^k dh \frac{h^2}{k^3(\nu a)^2} \frac{1}{|H_n^{(1)}(\nu a)|^2}
$$
$$
+ \frac{6}{\pi^2} \sum_{n=-\infty}^{\infty} \int_0^k dh \frac{n^2}{k(\nu a)^4} \frac{1}{|(d/dz)[H_n^{(1)}(z)]|_{z=\nu a}|^2}.
$$
$$
\qquad (22)
$$

Moreover, when the cylinder radius tends to zero, the decay rate of a radially oriented dipole tends to infinity. In the limit $ka = kb \to 0$, the main contribution to Eq. (22) is due to the TM mode with $n = 0$:

$$
\left(\frac{\gamma}{\gamma_0} \right)_{\mathrm{dip},\rho \; kb=ka\to 0} \sim \frac{3}{2(ka)^2} \left[1 + \frac{2}{\pi} \arctan(L^*) + \frac{4(\ln 2 - 1)}{\pi^2(1 + L^{*2})} + \cdots \right] + 4 + \cdots,
$$

$$
L^* = \frac{2}{\pi} \left[\ln \left(\frac{ka}{2} \right) + \gamma \right]. \qquad (23)
$$

In Eq. (23) $\gamma = 0.5772$ is the Euler constant.

III. QUADRUPOLE (FORBIDDEN) TRANSITIONS NEAR AN IDEALLY CONDUCTING CYLINDER

To investigate the quadrupole transitions near a cylinder one should first set an appropriate distribution of the charges and currents. It is well known [15] that generally the electric quadrupole momentum can be described as a traceless symmetric tensor D_{ij}. The definition of this tensor is

$$
D_{ij} = \int d\mathbf{r} \rho(\mathbf{r})(3 r_i r_j - \delta_{ij} r^2) \qquad (24a)
$$

within the classical approach and

$$
D_{ij} = \langle \psi_{\mathrm{out}} | (3 \hat{r}_i \hat{r}_j - \delta_{ij} \hat{r}^2) | \psi_{\mathrm{m}} \rangle \qquad (24b)
$$

within the quantum picture.

In any case, this tensor can be fixed by setting its five independent components. It is known [16] that, when considering quadrupole radiation, any charge and current distribution can be represented by a system of two dipoles of opposite orientations with the moments $e\mathbf{d}_1$ and $-e\mathbf{d}_1$, one of which is stationary and the other, displaced for a distance of $\delta\mathbf{r}(t)$, oscillating about the first. We consider such a system
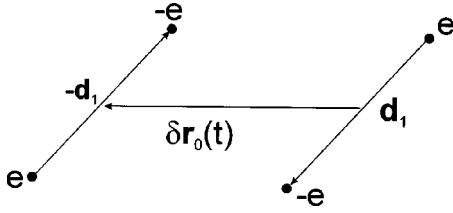
FIG. 2. Structure of quadrupole.

placed close to an ideally conducting cylinder of radius a in vacuum. The geometry of the classical problem is shown in Figs. 1 and 2.

The equation of motion of the movable dipole portion of the quadrupole in the case of a weak radiation reaction has the form

$$m\,\delta\ddot{\mathbf{r}} + m\,\gamma_{Q,0}\delta\dot{\mathbf{r}} + m\,\omega_0^2\,\delta\mathbf{r} = \mathbf{0}. \qquad (25)$$

Here

$$\gamma_{Q,0} = \frac{2e^2 d_1^2}{15c}\frac{k^4}{m} \qquad (26)$$

is the total quadrupole transition linewidth in vacuum.

An oscillating dipole located near a cylinder is acted upon additionally (compared to the case of free space) by the reflected field $\mathbf{E}^{(1)}(\mathbf{r}')$, so that the equation of motion assumes the form

$$m\,\delta\ddot{\mathbf{r}} + m\,\gamma_{Q,0}\delta\dot{\mathbf{r}} + m\,\omega_0^2\,\delta\mathbf{r} = -e(\mathbf{d}_1\cdot\boldsymbol{\nabla})\mathbf{E}^{(1)}(\mathbf{r}'). \quad (27)$$

By solving in accordance with perturbation theory the dispersion equation following from Eq. (27), one can easily find the formulas for the linewidth variation [4],

$$\gamma_Q = \gamma_{Q,0} - \frac{e}{\omega_0 m\,\delta r_0^2}\,\mathrm{Im}\{\delta\mathbf{r}_0\cdot[(\mathbf{d}_1\cdot\boldsymbol{\nabla}')\mathbf{E}^{(1)}(\mathbf{r}')]\}, \qquad (28)$$

where δr_0 is the oscillation amplitude of the moving dipole. Using Eq. (26), one can write the following expressions for the relative quantities:

$$\frac{\gamma_Q}{\gamma_{Q,0}} = 1 - \frac{15}{2e\,\delta\mathbf{r}_0^2 d_1^2 k^5}\,\mathrm{Im}\{\delta\mathbf{r}_0\cdot[(\mathbf{d}_1\cdot\boldsymbol{\nabla})E^{(1)}(\mathbf{r}')]\}. \qquad (29)$$

Thus, to get concrete results, one should calculate $\delta\mathbf{r}_0\cdot[(\mathbf{d}_1\cdot\boldsymbol{\nabla}')\mathbf{E}^{(1)}(\mathbf{r}')]$ at the location of the oscillating dipole. To do this one should solve the Maxwell's equations for the system of charges under analysis.

The charge density of the stationary dipole may be defined by the expression

$$\rho_1 = -e(\mathbf{d}_1\cdot\boldsymbol{\nabla})\,\delta(\mathbf{r}-\mathbf{r}') \qquad (30)$$

and that of the oscillating dipole by the expression

$$\rho_2 = e(\mathbf{d}_1\cdot\boldsymbol{\nabla})\,\delta(\mathbf{r}-\mathbf{r}'-\delta\mathbf{r}(t)). \qquad (31)$$

Accordingly, the total charge and current densities may be defined by the expressions

$$\rho_{\mathrm{tot}} = -e(\delta\mathbf{r}\cdot\boldsymbol{\nabla})(\mathbf{d}_1\cdot\boldsymbol{\nabla})\,\delta(\mathbf{r}-\mathbf{r}'), \qquad (32)$$

$$\mathbf{j} = e\mathbf{v}(t)(\mathbf{d}_1\cdot\boldsymbol{\nabla})\,\delta(\mathbf{r}-\mathbf{r}'), \quad \mathbf{v}(t) = \delta\dot{\mathbf{r}}(t). \qquad (33)$$

The solution of Maxwell's equations with a quadrupole source of the general kind (32) and (33) can be found by the substitution of Eqs. (32) and (33) into Eqs. (8) and (9). In the present paper, for simplicity, we will assume that $\mathbf{d}_1$ is parallel to $\delta\mathbf{r}(t)$, i.e., $\mathbf{d}_1\|\delta\mathbf{r}(t)$. In this case the quadrupole momentum tensor will be described by four rather than five independent components. Three of these components describe the orientation of tensor eigenaxes, while the fourth component is the magnitude of the quadrupole momentum D_0 [17]. Let us to recall that in the frame of eigenaxes the tensor of the quadrupole momentum has the following form:

$$\begin{bmatrix} -D_0/2 & 0 & 0 \\ 0 & -D_0/2 & 0 \\ 0 & 0 & D_0 \end{bmatrix}. \qquad (34)$$

In our case, when $\mathbf{d}_1\|\delta\mathbf{r}(t)$, $D_0 = -4e\,\delta r_0 d_1$, and the spontaneous linewidth of the quadrupole takes the form

$$\gamma_{Q,0} = \frac{cD_0^2 k^6}{240E_0}, \qquad (35)$$

where $E_0 = m\omega_0^2\,\delta r_0^2/2 = \hbar\omega_0$ is the total initial oscillation energy of the quadrupole.

Substituting Eqs. (32) and (33) with $\mathbf{d}_1\|\delta\mathbf{r}(t)$ into Eqs. (8) and (9) and integrating by parts, one can find the components of the electric field that we need. To calculate the linewidth for a φ-oriented axis of the quadrupole one should use the covariant derivative over φ [18] in Eq. (29):

$$\boldsymbol{\nabla}_\varphi E_\varphi = \frac{1}{\rho}\frac{\partial E_\varphi}{\partial\varphi} + \frac{E_\rho}{\rho}. \qquad (36)$$

As a result of using Eq. (29), the final expression for the relative rate of quadrupole transitions of an atom placed at $\mathbf{r}' = (\rho' = b, \varphi' = 0, z' = 0)$ near an ideally conducting cylinder takes the following form:

$$\frac{\gamma_Q}{\gamma_{Q,0}} = 1 - \tfrac{15}{2}\,\mathrm{Re}(W). \qquad (37)$$

In the case of ρ and φ orientations of the quadrupole, both TM and TE modes give contributions to the decay rate:

$$W_\rho = \sum_{n=-\infty}^{\infty}\int_0^k dh\,\frac{h^2\nu^2}{k^5}\left(\frac{d^2}{dz^2}[H_n^{(1)}(z)]\bigg|_{z=\nu b}\right)^2 \frac{J_n(\nu a)}{H_n^{(1)}(\nu a)}$$
$$+ \sum_{n=-\infty}^{\infty}\int_0^k dh\,\frac{\nu^2 n^2}{k^3}\left[\frac{d}{dz}\left(\frac{H_n^{(1)}(z)}{z}\right)\bigg|_{z=\nu b}\right]^2$$
$$\times \frac{(d/dz)[J_n(z)]|_{z=\nu a}}{(d/dz)[H_n^{(1)}(z)]|_{z=\nu a}}, \qquad (38)$$

$$W_\varphi = \sum_{n=-\infty}^{\infty} \int_0^k dh \frac{h^2}{k(kb)^4 \nu^2} \frac{J_n(\nu a)}{H_n^{(1)}(\nu a)} \left(\nu b \right.$$

$$\times \frac{d}{dz}[H_n^{(1)}(z)]\bigg|_{z=\nu b} - n^2 H_n^{(1)}(\nu b) \bigg)^2$$

$$+ \sum_{n=-\infty}^{\infty} \int_0^k dh \frac{n^2 \nu^2}{k^3} \frac{(d/dz)[J_n(z)]|_{z=\nu a}}{(d/dz)[H_n^{(1)}(z)]|_{z=\nu a}}$$

$$\times \left[\frac{d}{dz}\left(\frac{H_n^{(1)}(z)}{z}\right) \bigg|_{z=\nu b} \right]^2. \tag{39}$$

In the case of z orientation only the TM modes give contributions to the decay rate:

$$W_z = \sum_{n=-\infty}^{\infty} \int_0^k dh \frac{\nu^2 h^2}{k^5} \frac{[H_n^{(1)}(\nu b)]^2 J_n(\nu a)}{H_n^{(1)}(\nu a)}. \tag{40}$$

In all these cases $\nu = \sqrt{k^2 - h^2}$ is the radial wave number.

The expressions (37)–(40) have a form that is useful for some analytical investigations. However, it is difficult to recognize from Eqs. (37)–(40) that decay rates are positive quantities. If one calculates decay rates within the quantum approach through Fermi's golden rule, it is possible to obtain instead of Eqs. (37)–(40) the explicitly positive expressions (for details see the Appendix)

$$\frac{\gamma_{Q,\rho}}{\gamma_{Q,0}} = \frac{15}{2} \sum_{n=-\infty}^{\infty} \int_0^k dh \frac{h^2 \nu^2}{k^5} \left[\frac{d^2}{dz^2}[J_n(z)] \right|_{z=\nu b}$$

$$- \frac{J_n(\nu a)}{H_n^{(1)}(\nu a)} \frac{d^2}{dz^2}[H_n^{(1)}(z)] \bigg|_{z=\nu b} \bigg]^2$$

$$+ \frac{15}{2} \sum_{n=-\infty}^{\infty} \int_0^k dh \frac{\nu^2 n^2}{k^3} \left[\frac{d}{dz}\left(\frac{J_n(z)}{z}\right) \right|_{z=\nu b}$$

$$- \frac{(d/dz)[J_n(z)]|_{z=\nu a}}{(d/dz)[H_n^{(1)}(z)]|_{z=\nu a}} \frac{d}{dz}\left(\frac{H_n^{(1)}(z)}{z}\right) \bigg|_{z=\nu b} \bigg]^2, \tag{41}$$

$$\frac{\gamma_{Q,\varphi}}{\gamma_{Q,0}} = \frac{15}{2} \sum_{n=-\infty}^{\infty} \int_0^k dh \frac{h^2}{k(kb)^4 \nu^2} \left[\left(z \frac{d}{dz} J_n(z) - n^2 J_n(z) \right) \right|_{z=\nu b}$$

$$- \frac{J_n(\nu a)}{H_n^{(1)}(\nu a)} \left(z \frac{d}{dz} H_n^{(1)}(z) - n^2 H_n^{(1)}(z) \right) \bigg|_{z=\nu b} \bigg]^2$$

$$+ \frac{15}{2} \sum_{n=-\infty}^{\infty} \int_0^k dh \frac{n^2 \nu^2}{k^3} \left[\frac{d}{dz}\left(\frac{J_n(z)}{z}\right) \right|_{z=\nu b}$$

$$- \left[\frac{(d/dz)[J_n(z)]|_{z=\nu a}}{(d/dz)[H_n^{(1)}(z)]|_{z=\nu a}} \frac{d}{dz}\left(\frac{H_n^{(1)}(z)}{z}\right) \bigg|_{z=\nu b} \right] \bigg]^2, \tag{42}$$

$$\frac{\gamma_{Q,z}}{\gamma_{Q,0}} = \frac{15}{2} \sum_{n=-\infty}^{\infty} \int_0^k dh \frac{\nu^2 h^2}{k^5}$$

$$\times \left| J_n(\nu b) - \frac{J_n(\nu a)}{H_n^{(1)}(\nu a)} H_n^{(1)}(\nu b) \right|^2. \tag{43}$$

Using the identities

$$\sum_{n=-\infty}^{n=\infty} \left(z \frac{d}{dz} J_n(z) - n^2 J_n(z) \right)^2 = \frac{3z^4}{8},$$

$$\sum_{n=-\infty}^{n=\infty} n^2 \left[\frac{d}{dz}\left(\frac{J_n(z)}{z}\right) \right]^2 = \frac{1}{8},$$

$$\sum_{n=-\infty}^{n=\infty} \left(\frac{d^2 J_n(z)}{dz^2} \right)^2 = \frac{3}{8},$$

one can show the equivalence of Eqs. (37)–(40) and Eqs. (41)–(43), i.e., the equivalence of the classical and quantum approaches.

From Eqs. (37)–(40) it is easy to see that when an atom has moved to infinity ($b \rightarrow \infty$) the reflected field tends to zero and the radiative linewidth tends to the free-space value. The behavior of these rates becomes more interesting as the atom approaches the cylinder surface ($b \rightarrow a$). In this case it is possible to show from Eq. (43) that the transition rate for z orientation of the quadrupole tends to zero for any radius of cylinder. On the other hand, the decay rates for quadrupoles with ρ and φ orientations do not vanish when the atom is placed on the cylinder surface ($b = a$):

$$\frac{\gamma_{Q,\rho}}{\gamma_{Q,0}} = \frac{\gamma_{Q,\varphi}}{\gamma_{Q,0}} = \frac{30}{\pi^2 (ka)^2} \sum_{n=-\infty}^{\infty} \int_0^k dh \frac{h^2}{k^3 (\nu a)^2} \frac{1}{|H_n^{(1)}(\nu a)|^2}$$

$$+ \frac{30}{\pi^2 (ka)^2} \sum_{n=-\infty}^{\infty} \int_0^k$$

$$\times dh \frac{n^2}{k(\nu a)^4} \frac{1}{|(d/dz)[H_n^{(1)}(z)]|_{z=\nu a}|^2}. \tag{44}$$

It is interesting to note that the decay rates for ρ and φ orientations become equal. Moreover, these quadrupole decay rates have a simple relation to the dipole decay rate ($b = a$):

$$\frac{\gamma_{Q,\rho}}{\gamma_{Q,0}} = \frac{\gamma_{Q,\varphi}}{\gamma_{Q,0}} = \frac{5}{(ka)^2} \frac{\gamma_{dip,\rho}}{\gamma_{dip,0}}. \tag{45}$$

When the cylinder radius tends to zero, the decay rates of quadrupole with these orientations tend to infinity. In the limit $ka = kb \rightarrow 0$ the main contributions to Eqs. (44) and (45) are due to the TM mode with $n = 0$:
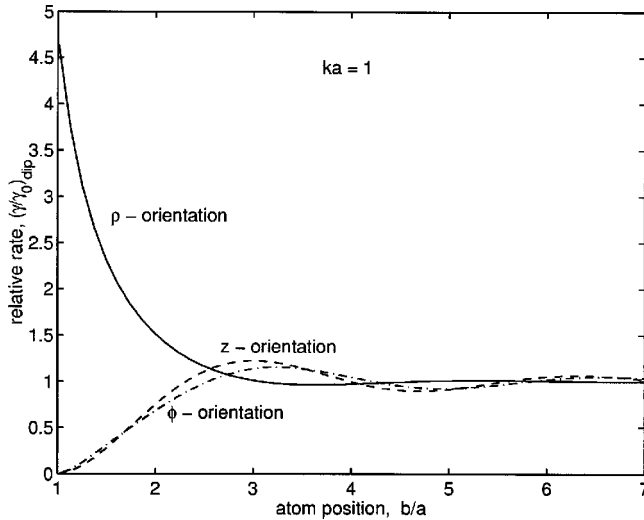
FIG. 3. Relative linewidth of dipole transitions for various orientations as a function of the distance b/a to the surface of a metal cylinder ($ka=1$).

FIG. 4. Relative linewidth of quadrupole transitions for various orientations as a function of the distance b/a to the surface of a metal cylinder ($ka=1$).

$$\left(\frac{\gamma}{\gamma_0}\right)_{Q,\rho} = \left(\frac{\gamma}{\gamma_0}\right)_{Q,\varphi} \underset{kb=ka\to 0}{\sim} \frac{15}{2(ka)^4}$$

$$\times \left(1 + \frac{2}{\pi}\arctan(L^*) + \frac{4(\ln 2 - 1)}{\pi^2(1+L^{*2})} + \cdots\right)$$

$$+ \frac{20}{(ka)^2} + \cdots, \tag{46}$$

$$L^* = \frac{2}{\pi}\left[\ln\left(\frac{ka}{2}\right) + \gamma\right].$$

In Eq. (44) $\gamma = 0.5772$ is the Euler constant.

IV. ANALYSIS OF RESULTS AND ILLUSTRATIONS

The expressions (15)–(23) and (37)–(46) are the main results of the present paper. In general, to calculate linewidths for specific parameters one should sum up an infinite series and perform integration of nontrivial Bessel functions (see Ref. [18], p. 5). When an atom is moved off to infinity ($b\to\infty$), these series are poorly convergent and it is necessary to make the Watson transformation [19,20] to treat the problem. However, this domain ($b\to\infty$) is not the most interesting, because the behavior of the linewidth is trivial.

One can expect the maximum influence of a cylinder on the linewidth when the atom is placed near its surface. Moreover, specific features can be observed when the cylinder radius is small ($ka\lesssim 10$).

The results of our calculations for dipole (allowed) transitions with different orientations of momentum are shown in Fig. 3. From this figure one can observe the qualitative difference between radial (ρ) and tangential (φ,z) orientations of the dipole. The behavior of the linewidth for tangential orientations is simple: at $b=a$ (atom located on the cylinder surface) there is no radiation at all and the linewidth is zero.
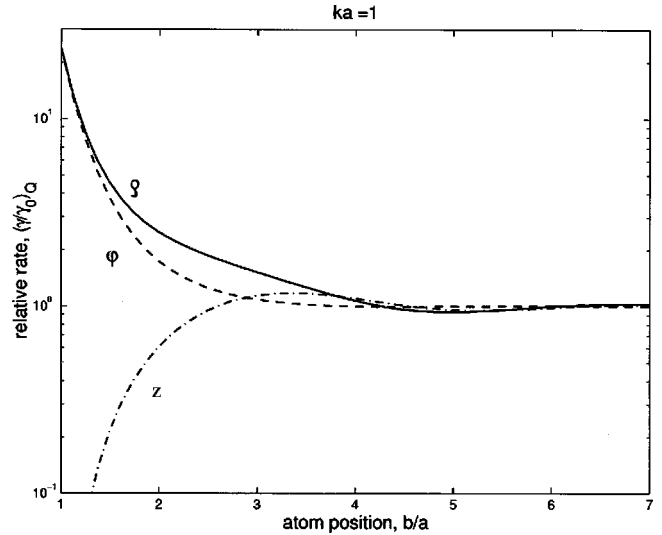
With further increase of b, the relative linewidths tend to unity with small oscillations.

The behavior of the linewidth for radial orientations is more interesting. At $b=a\to 0$, the increase of decay rates diverges like

$$\frac{\gamma_{\text{dip},\rho}}{\gamma_{\text{dip},0}} \propto \frac{1}{(ka)^2}. \tag{47}$$

The behavior of decay rates for forbidden (quadrupole) transitions is shown in Fig. 4, for different orientations of the quadrupole axis. For z orientations the decay rate of an atom placed on the cylinder surface $b=a$ is equal to zero for any radius of cylinder. When a quadrupole moves off the surface to infinity, the quadrupole decay rate approaches the free-space value with small oscillations. This case is analogous to that of a z-oriented dipole. The behavior of the quadrupole decay rate for ρ and φ orientations is more interesting. When an atom is placed near the surface of the cylinder ($b\to a$) the quadrupole decay rates do not vanish. Moreover, the decay rates associated with such transitions tend to infinity when the cylinder radius tends to zero, $a\to 0$. According to Eq. (46) these rates increase like

$$\frac{\gamma_{Q,\rho}}{\gamma_{Q,0}} \propto \frac{1}{(ka)^4} \tag{48}$$

which is more singular than in the dipole case [Eq. (45)].

In Fig. 5 the behavior of transition rates and their asymptotes at $b=a\to 0$ is shown. In this figure one can see the unbounded increase of rates. One can also observe here the good agreement between the exact expressions (16) and (38) and their asymptotes (23) and (46). Note, that according to Eqs. (44) and (45) the quadrupole decay rates with φ orientation are no different from those for ρ orientation.

According to Eq. (46) and Fig. 5, the relative decay rates of quadrupoles increase much faster than those of dipoles at
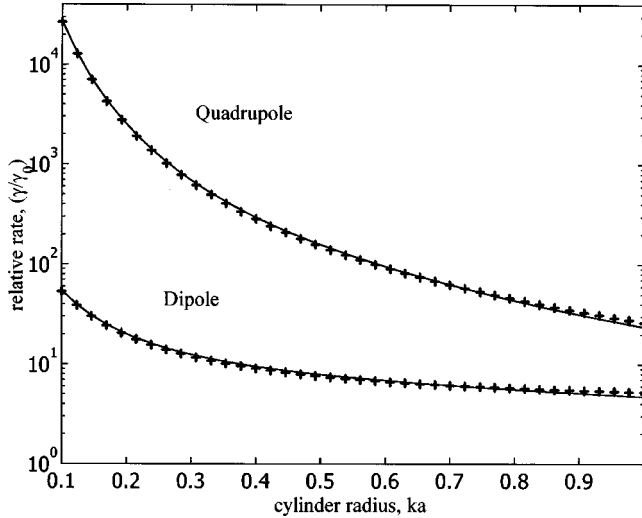
FIG. 5. Relative linewidth for quadrupole and dipole transitions in atoms located in close proximity to the surface of a metal cylinder ($b=a$) in the case of radial orientation as a function of the cylinder radius ka. The crosses indicate asymptotic relations (23) and (46).

$ka=kb\to0$. So it is of interest to find the ratio of the absolute values of the rates. From Eq. (45) it is easy to find that

$$\frac{\gamma_{Q,\rho}}{\gamma_{\text{dip},\rho}}=\frac{5}{(ka)^2}\frac{\gamma_{Q,0}}{\gamma_{\text{dip},0}}. \tag{49}$$

It is well known [1] that the quadrupole decay rate is suppresed by the factor $(ka_0)^2$ in comparison with the dipole decay rate (where a_0 is the Bohr radius). As a result we get instead of Eq. (49) the estimation

$$\frac{\gamma_{Q,\rho}}{\gamma_{\text{dip},\rho}}\propto5\left(\frac{a_0}{a}\right)^2. \tag{50}$$

For example, in the case of an atom located near a conducting carbon nanotube [21,22] with $a\approx5$ Å we have a significant enhancement of the quadrupole transition rates:

$$\frac{\gamma_{Q,\rho}}{\gamma_{\text{dip},\rho}}\propto10^{-2}. \tag{51}$$

The singular behavior of dipole rates with ρ orientation and quadrupole rates with ρ, φ orientations differs substantially from the behavior of rates near an ideally conducting sphere or plane. In the case of an ideally conducting plane, the expressions for dipole decay rates have the following form [2]:

$$\frac{\gamma_{\text{dip},\perp}}{\gamma_{\text{dip},0}}=1-3\frac{\cos2x}{(2x)^2}+3\frac{\sin2x}{(2x)^3}, \tag{52}$$

$$\frac{\gamma_{\text{dip},\parallel}}{\gamma_{\text{dip},0}}=1-\frac{3}{2}\left(\frac{\sin2x}{2x}+\frac{\cos2x}{(2x)^2}-\frac{\sin2x}{(2x)^3}\right). \tag{53}$$

Here $x=k(b-a)$ is the dimensionless distance between atom and surface. Here and elsewhere we use the symbols $\perp$ and $\parallel$ for orientations that are normal and tangential to the surface.

In the case of quadrupole transitions with $\mathbf{d}_1\|\delta\mathbf{r}(t)$ one can show that the expressions for the decay rate have a similar form although the singularity of different terms is higher:

$$\frac{\gamma_{Q,\perp}}{\gamma_{Q,0}}=1+\frac{15}{8}\sin2x\left(\frac{3}{x^5}-\frac{5}{x^3}\right)+\frac{15}{4}\cos2x\left(\frac{1}{x^2}-\frac{3}{x^4}\right), \tag{54}$$

$$\frac{\gamma_{Q,\parallel}}{\gamma_{Q,0}}=1+\frac{15}{64}\sin2x\left(\frac{9}{x^5}-\frac{16}{x^3}\right)+\frac{15}{32}\cos2x\left(\frac{4}{x^2}-\frac{9}{x^4}\right). \tag{55}$$

In the domain of small $x\to0$ we obtain for the dipole

$$\frac{\gamma_{\text{dip},\perp}}{\gamma_{\text{dip},0}}=2,\quad\frac{\gamma_{\text{dip},\parallel}}{\gamma_{\text{dip},0}}=0, \tag{56}$$

and for the quadrupole

$$\frac{\gamma_{Q,\perp}}{\gamma_{Q,0}}=\frac{\gamma_{Q,\parallel}}{\gamma_{Q,0}}=0. \tag{57}$$

From these expressions one can see that in the case of a plane interface only the dipole with radial orientation has a nonzero decay rate when placed on a surface. Moreover, there are no conditions when the decay rate tends to infinity. The decay rates for a cylinder of infinite radius ($ka\to\infty$) agree, of course, with the rates (56) and (57).

The spherical geometry case has an intermediate position between cylindrical and plane interfaces, if one makes a classification by degree of singularity of decay rates. In the case of spherical geometry, for a dipole placed at $r=b$ near an ideally conducting sphere of radius a, we have [23]

$$\frac{\gamma_{\text{dip},\perp}}{\gamma_{\text{dip},0}}=1-\frac{3}{2}\text{Re}\left[\sum_{n=1}^{\infty}n(n+1)(2n+1)q_n\left(\frac{h_n^{(1)}(z)}{z}\right)^2\right]_{z=kb}, \tag{58}$$

$$\frac{\gamma_{\text{dip},\parallel}}{\gamma_{\text{dip},0}}=1-\frac{3}{2}\text{Re}\left[\sum_{n=1}^{\infty}(n+\tfrac{1}{2})\left\{p_n[h_n^{(1)}(z)]^2+q_n\left(\frac{d[zh_n^{(1)}(z)]}{z\,dz}\right)^2\right\}\right]_{z=kb} \tag{59}$$

where p_n and q_n are Mie coefficients for an ideally conducting sphere:

$$q_n=\frac{(d/dz_2)[z_2j_n(z_2)]}{(d/dz_2)[z_2h_n^{(1)}(z_2)]}\Bigg|_{z_2=ka}, \tag{60}$$

$$p_n=\frac{j_n(z_2)}{h_n^{(1)}(z_2)}\Bigg|_{z_2=ka}. \tag{61}$$

TABLE I. Dipole decay rates for different geometries and orientations. Atom is on the surface ($a=b$, $ka\rightarrow0$).

Orientation	Geometry		
	Plane	Sphere	Cylinder
Perpendicular to surface	2	9	$\dfrac{3}{2(ka)^2}$
Parallel to surface (φ)	0	0	0
Parallel to surface (z)	0	0	0

TABLE II. Quadrupole decay rates for different geometries and orientations. Atom is on the surface ($a=b$, $ka\rightarrow0$).

Orientation	Geometry		
	Plane	Sphere	Cylinder
Perpendicular to surface	0	$\dfrac{180}{(ka)^2}$	$\dfrac{15}{2(ka)^4}$
Parallel to surface (φ)	0	$\dfrac{45}{(ka)^2}$	$\dfrac{15}{2(ka)^4}$
Parallel to surface (z)	0	$\dfrac{45}{(ka)^2}$	0

In the case of a quadrupole with $\mathbf{d}_1\|\delta\mathbf{r}(t)$ the decay rates take the form [4,5]

$$\frac{\gamma_{Q,\perp}}{\gamma_{Q,0}}=1-\frac{15}{2}\sum_{n=1}^{\infty}n(n+1)(2n+1)$$
$$\times\mathrm{Re}\left\{q_n\left[\frac{d}{dz}\left(\frac{h_n^{(1)}(z)}{z}\right)\right]^2\right\}_{z=kb},\qquad(62)$$

$$\frac{\gamma_{Q,\|}}{\gamma_{Q,0}}=1-\frac{15}{8}\sum_{n=1}^{\infty}n(n+1)(2n+1)$$
$$\times\mathrm{Re}\left\{q_n\left[\frac{d}{dz}\left(\frac{h_n^{(1)}(z)}{z}\right)\right]^2\right\}_{z=kb}-\frac{15}{16}\sum_{n=1}^{\infty}(n-1)$$
$$\times(n+2)(2n+1)\mathrm{Re}\left\{q_n\left[\frac{1}{z^2}\frac{d}{dz}[zh_n^{(1)}(z)]\right]^2\right\}_{z=kb}$$
$$-\frac{15}{16}\sum_{n=1}^{\infty}(n-1)(n+2)(2n+1)$$
$$\times\mathrm{Re}\left(p_n\left[\frac{1}{z}[h_n^{(1)}(z)]\right]^2\right)_{z=kb}.\qquad(63)$$

In the case of an atom placed on the surface of an ideally conducting metal sphere whose radius tends to zero, one can obtain for dipole transitions

$$\frac{\gamma_{\mathrm{dip},\perp}}{\gamma_{\mathrm{dip},0}}=9,\quad\frac{\gamma_{\mathrm{dip},\|}}{\gamma_{\mathrm{dip},0}}=0.\qquad(64)$$

In the case of quadrupole transitions, the decay rates tend to infinity in all cases:

$$\frac{\gamma_{Q,\perp}}{\gamma_{Q,0}}=\frac{180}{(ka)^2}+\cdots,\quad\frac{\gamma_{Q,\|}}{\gamma_{Q,0}}=\frac{45}{(ka)^2}+\cdots.\qquad(65)$$

From Eqs. (64) and (65) one can see that dipole transition rates are limited (as in the case of plane geometry) while both radial and tangential rates of quadrupole transitions have the singularities $1/(ka)^2$ at $kb=ka\rightarrow0$.

To summarize the situation, we put together asymptotic expressions and limits for the dipole transitions in Table I and for the quadrupole transitions in Table II. From these tables it is easy to see that in general a transition near a cylinder of small enough radius ($ka\rightarrow0$) has a higher decay

rate than near a plane or sphere. The only exception is for the z orientation of a quadrupole when the decay rate near the cylinder is equal to 0.

In Figs. 6 and 7 the behavior of transition rates in the case of radial orientations of dipole and quadrupole moments for different geometries is shown. The singular behavior at $ka\rightarrow0$ described above is clear in these figures. From Tables I and II it is easy to find that to achieve the asymptotic regime the radius of cylinder and sphere should satisfy the relation

$$\frac{3}{2(ka)^2}>9\quad\text{or}\quad ka<\frac{1}{\sqrt{6}}\quad\text{(dipole case)}$$

and

$$\frac{15}{2(ka)^4}>\frac{180}{(ka)^2}\quad\text{or}\quad ka<\frac{1}{2\sqrt{6}}\quad\text{(quadrupole case)}.$$

The substantial difference between the singular asymptotes of decay rates for the cylinder and sphere is due to the fact that a dipole or quadrupole placed near a cylinder generates surface current, which slowly decreases along the z
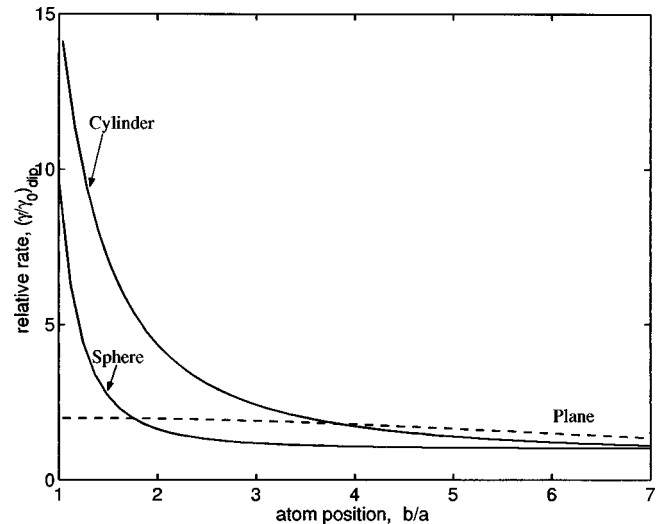
FIG. 6. Relative linewidth of dipole transitions for different geometries as a function of the distance b/a to the surface of a metal cylinder ($ka=0.25$, radial orientation).
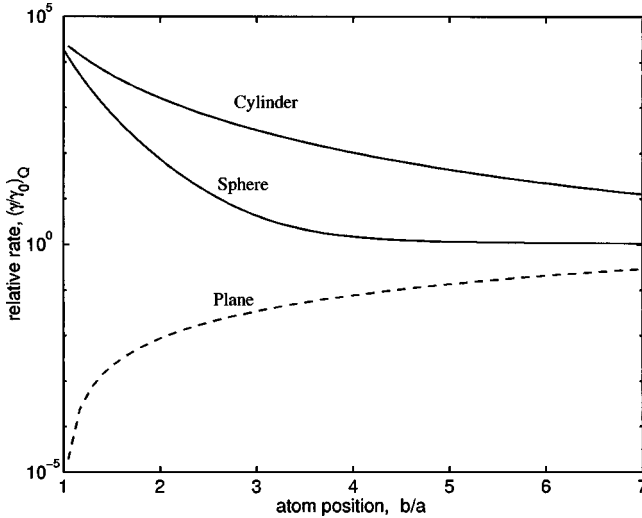
FIG. 7. Relative linewidth of quadrupole transitions for different geometries as a function of the distance b/a to the surface of a metal cylinder ($ka = 0.1$, radial orientation).

axis. The expression for the symmetrical part ($n=0$) of the total current I_z has the following form for a radial dipole placed on the surface of a cylinder:

$$I_z = \frac{ac}{2} H_\varphi(\rho = a) = \frac{-icd_0 k}{\pi} \int_0^\infty dh \frac{h}{\nu} \sin(hz) \frac{H_1^{(1)}(\nu a)}{H_0^{(1)}(\nu a)},$$

$$(66)$$

$$\mathrm{Re} I_z = \frac{-2cd_0 k}{\pi^2 a} \int_0^k dh \frac{h}{\nu^2} \frac{\sin(hz)}{|H_0^{(1)}(\nu a)|^2}.$$

In Fig. 8 the dependence of the real part of current (66), $\mathrm{Re}\, I_z$, on the radius of the cylinder a and distance along the z axis is shown. From this figure one can see that current amplitude increases when the cylinder radius tends to zero. As a result the radiation power and decay rate are increasing.

In other words, the cylinder is an antenna, which is effectively excited by a dipole or quadrupole oscillator. The high efficiency of antenna excitation is due to the fact that the
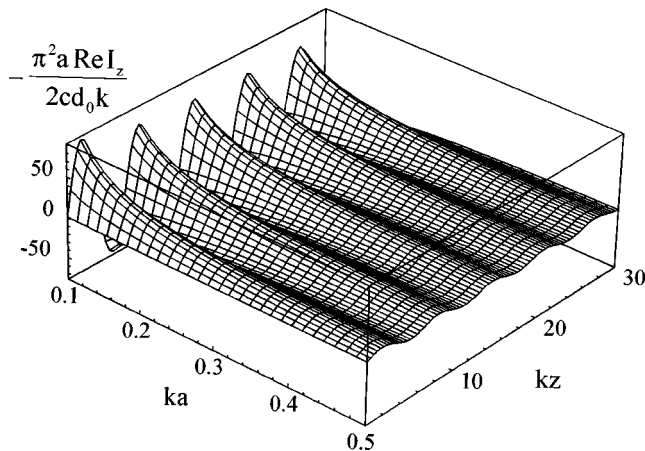
FIG. 8. The dependence of the real part of Eq. (66) on cylinder radius and distance along z axis. Radial dipole oscillates on the surface of cylinder ($b=a$).

radiation pattern of dipole and quadrupole radiation with ρ and φ orientations has a maximum along the z direction.

V. CONCLUSION

In the present paper the behavior of dipole and quadrupole transitions in an atom placed near an ideally conducting cylindrical surface was considered. Explicit analytical expressions for transition rates for different orientations of dipole and quadrupole were found. It was shown that the rates of both dipole and quadrupole transition with radial orientation of the moments tend to infinity when the cylinder radius tends to zero. The degree of singularity for the quadrupole rate is higher in comparison with the dipole rate. As to φ orientation, the dipole decay rate decreases when the atom is placed near a surface, while the quadrupole rate may increase infinitely if the cylinder radius tends to zero. Such behavior has analogy in neither plane nor spherical interface geometry.

Such a behavior of the decay rates is connected with effective excitation of surface waves, which absorb dipole energy and then radiate it. In the spherical case such waves are not excited and the degree of singularity is lower here. Because of these distinctions between spherical and cylindrical geometries, consideration of the problem of allowed and forbidden transitions is of great interest within geometry which can be both spherical and cylindrical (e.g., a prolate ellipsoid of rotation).

In the present paper we have dealt with the case of an axis-symmetric distribution of currents in a radiating quadrupole. That is why the investigation of radiation of an arbitrary quadrupole (and magnetic dipole) is also of interest.

Another important direction for investigation is the study of allowed and forbidden transitions near a dielectric fiber of small radius. Here we expect a number of different effects, because the modes propagating without attenuation (waveguided modes) exist in a dielectric cylinder of any shape and size. There are no such modes near an ideally conducting cylinder.

To test our predictions experimentally one can try to measure the fluorescence from excited atoms moving near a dielectric or conducting cylinder. Optical fibers or the usual wires of submicrometer diameter can be considered as such cylinders. However, to enhance the effects one can try to use instead single-wall carbon nanotubes [21,22]. These bodies have the form of a cylinder with radius of the order 5 Å and they may be metallic or semiconducting with a wide gap depending on structure. These and related items are under active investigation now.

APPENDIX: QUANTUM THEORY OF RADIATION OF AN ATOM PLACED NEAR AN IDEALLY CONDUCTING CYLINDER

By and large the procedure for calculation of dipole and quadrupole decay rates near a cylinder is similar to the case of a dielectric microsphere [4]. To quantize the electromagnetic field it is convenient to place the cylinder inside a large cavity. In our problem, the cavity may be taken in the form of an ideally conducting cylinder of finite but large radius $\Lambda \to \infty$ and length $L \to \infty$. Essentially the system cylinder+cavity will form a coaxial resonator. The final results will be independent of Λ and L.

The expansion of the electromagnetic field and its vector potential over the complete set of eigenfunctions of the classical problem (standing cylindrical waves) may be represented in the form

$$\hat{\mathbf{E}} = \sum_s \frac{a_s \mathbf{e}(s,\mathbf{r}) - a_s^\dagger \mathbf{e}^*(s,\mathbf{r})}{i\sqrt{2}},$$

$$\hat{\mathbf{B}} = \sum_s \frac{a_s \mathbf{b}(s,\mathbf{r}) + a_s^\dagger \mathbf{b}^*(s,\mathbf{r})}{\sqrt{2}}, \qquad (A1)$$

$$\hat{\mathbf{A}} = -\sum_s \frac{c}{\omega_s} \frac{a_s \mathbf{e}(s,\mathbf{r}) + a_s^\dagger \mathbf{e}^*(s,\mathbf{r})}{\sqrt{2}}.$$

Here a_s and $a_s^\dagger$ are the photon annihilation and creation operators in the corresponding modes with ordinary commutation relations, and ω_s are the frequencies of these modes. The vector index s includes the mode type (TE or TM) and a set of quantum numbers (see below).

In our case the Maxwell's equations defining photon wave functions have the form

$$\nabla \times \mathbf{e}(s,\mathbf{r}) = -\frac{\omega_s}{c} \mathbf{b}(s,\mathbf{r}),$$

$$\qquad (A2)$$

$$\nabla \times \mathbf{b}(s,\mathbf{r}) = -\frac{\omega_s}{c} \mathbf{e}(s,\mathbf{r}).$$

Notice that for our choice of mode functions $\mathrm{div}(\hat{\mathbf{E}}) = \mathrm{div}(\hat{\mathbf{A}}) = 0$. We also assume that the photon wave functions are normalized to 1 in a quantization volume. As a result the wave functions should satisfy the following conditions:

$$\frac{1}{4\pi} \int d\mathbf{r}\, \mathbf{e}^*(s,\mathbf{r}) \cdot \mathbf{e}(s',\mathbf{r}) = \delta_{ss'} \hbar \omega_s,$$

$$\qquad (A3)$$

$$\frac{1}{4\pi} \int d\mathbf{r}\, \mathbf{b}^*(s,\mathbf{r}) \cdot \mathbf{b}(s',\mathbf{r}) = \delta_{ss'} \hbar \omega_s.$$

It is not very difficult to obtain expressions for the electric field strength $\mathbf{e}(s,\mathbf{r})$ of the sth TM mode in terms of Bessel functions [24]:

$$e_z = C_{\mathrm{TM}} \nu^2 [J_m(\nu\rho) - Y_m(\nu\rho) q_{\mathrm{TM}}(m,\nu a)] e^{im\varphi} \cos(hz),$$

$$e_\rho = -C_{\mathrm{TM}} \nu h [J_m'(\nu\rho) - Y_m'(\nu\rho) q_{\mathrm{TM}}(m,\nu a)] e^{im\varphi} \sin(hz),$$

$$\qquad (A4)$$

$$e_\varphi = \frac{-i C_{\mathrm{TM}} h m}{\rho} [J_m(\nu\rho) - Y_m(\nu\rho) q_{\mathrm{TM}}(m,\nu a)] e^{im\varphi} \sin(hz).$$

In Eq. (A4) the prime stands for the derivative, ν is the radial wave vector, h the longitudinal wave vector, and

$$q_{\mathrm{TM}}(m,\nu a) = \frac{J_m(\nu a)}{Y_m(\nu a)},$$

$$\qquad (A5)$$

$$C_{\mathrm{TM}} = \left(\frac{4\pi\hbar\omega_g}{L\Lambda\nu[1 + q_{\mathrm{TM}}(m,\nu a)^2] k^2} \right)^{1/2}.$$

The expression (A4) provides the fulfillment of boundary conditions for TM modes on the cylinder surface ($\rho = a$) at any h, ν. To satisfy boundary conditions on the surface of quantization volume it is necessary to impose the following conditions on h, ν:

$$h = \frac{\pi n_z}{L}, \quad n_z = 0,1,2,...,$$

$$\qquad (A6)$$

$$J_m(\nu\Lambda) - Y_m(\nu\Lambda) q_{\mathrm{TM}}(m,\nu a) = 0.$$

In the limit $\Lambda \to \infty$ the second equation has the asymptotic solution

$$\nu = \frac{\pi}{\Lambda}(n_\rho + m/2 + 1/4) + \cdots, \quad n_\rho = 0,1,2,... . \qquad (A7)$$

The quantum number set $\{m, n_z, n_\rho\}$ forms the vector index $s = \{m, n_z, n_\rho\}$ for the TM modes used above.

In the case of transverse electric modes the expressions for the electric fields have the following form [24]:

$$e_z = 0,$$

$$e_\rho = -\frac{C_{\mathrm{TE}} k m}{\rho} [J_m(\nu\rho) - Y_m(\nu\rho) q_{\mathrm{TE}}(m,\nu a)] e^{im\varphi} \sin(hz),$$

$$\qquad (A8)$$

$$e_\varphi = -i C_{\mathrm{TE}} k \nu [J_m'(\nu\rho) - Y_m'(\nu\rho) q_{\mathrm{TE}}(m,\nu a)] e^{im\varphi} \sin(hz),$$

where

$$q_{\mathrm{TE}}(m,\nu a) = \frac{J_m'(\nu a)}{Y_m'(\nu a)},$$

$$\qquad (A9)$$

$$C_{\mathrm{TE}} = \left(\frac{4\pi\hbar\omega_s}{L\Lambda\nu[1 + q_{\mathrm{TE}}(m,\nu a)^2] k^2} \right)^{1/2}.$$

The expression (A8) provides the fulfillment of boundary conditions for TE modes on the cylinder surface ($\rho = a$) at any h, ν. To satisfy boundary conditions on the surface of quantization volume it is necessary to impose the following conditions on h, ν:

$$h = \frac{\pi n_z}{L}, \quad n_z = 0,1,2,\ldots,$$

$$J'_m(\nu\Lambda) - Y'_m(\nu\Lambda)q_{\text{TE}}(m,\nu a) = 0. \tag{A10}$$

In the limit $\Lambda \to \infty$ the second equation has the asymptotic solution

$$\nu = \frac{\pi}{\Lambda}(n_\rho + m/2 + 1/4) + \cdots, \quad n_\rho = 0,1,2,\ldots. \tag{A11}$$

The quantum number set $\{m,n_z,n_\rho\}$ forms the vector index $s = (n,m,n)$ for the TE modes used above.

In the case of a coaxial resonator, there are so-called fundamental modes apart from the modes considered above. In our case, however, the fundamental modes give no contribution to dipole or quadrupole decay rates in the limit $\Lambda \to \infty$. In our case the frequencies of quantized modes are defined by the following relation:

$$\omega_s = c\sqrt{\nu^2 + h^2} \tag{A12}$$

where ν, h are defined by the quantization conditions (A6) and (A10).

To study the interaction between an atomic oscillator and the continuum of electromagnetic modes modified by the presence of a cylinder, it is also necessary to know the density of final states. From Eq. (A12) it is easy to find that the density of final states will be defined by the simple expression

$$\rho_{\text{TM}}(\omega) = \delta(\omega - \omega_s(n_z,n_\rho)) \frac{dn_z dn_\rho}{\hbar}$$

$$= \delta(\omega - c\sqrt{h^2 + \nu^2}) \frac{L\Lambda \, dh \, d\nu}{\pi^2 \hbar} = \frac{L\Lambda}{\pi^2 \hbar c} \frac{k}{\nu} dh. \tag{A13}$$

In deriving Eq. (A13), we changed from discrete variables n_z, n_ρ to continuous wave vectors h, ν in the usual way. As a result the longitudinal wave vector is the only independent variable, whereas the radial wave number is expressed by the relation $\nu = \sqrt{k^2 - h^2}$. In the case of TE modes we have the same density of final states.

The Hamiltonian of interaction of the atom with the electromagnetic field can be constructed in the usual way [2]. To calculate the dipole and quadrupole rates within the lowest order of perturbation theory, we need to keep only the following term from the full interaction Hamiltonian:

$$H_{\text{int}} = -\frac{e}{mc}\hat{\mathbf{A}}(\mathbf{r})\cdot\hat{\mathbf{p}} + \cdots. \tag{A14}$$

Here $\hat{\mathbf{A}}(\mathbf{r})$ is the vector potential operator at the electron position, $\hat{\mathbf{p}}$ is the momentum of the electron, and m is the electron mass.

Now, according to the golden rule the decay rates are given by [25]

$$\gamma = \frac{2\pi}{\hbar} \sum_{\text{final}} |\langle \text{initial}|H_{\text{int}}|\text{final}\rangle|^2 \rho(\omega) \tag{A15}$$

where the sum is over all final states. Notice that to obtain from Eq. (A15) the correct expressions for the decay rates of dipole as well as quadrupole transitions one should place an atom (which is placed at $\mathbf{r}_0$) far enough from the left wall of the quantization volume (which is at $z=0$). In other words, one should take the limit $z_0 \to \infty$ in Eq. (A15). This procedure is equivalent to the substitutions

$$\sin^2(hz) \to \tfrac{1}{2}, \quad \cos^2(hz) \to \tfrac{1}{2}, \quad \sin(hz)\cos(hz) \to 0. \tag{A16}$$

In the case of the dipole transitions it is easy to find from Eq. (A15) the decay rate

$$\gamma_{\text{dip}} = \frac{L\Lambda}{\pi\hbar^2 c}\left(\sum_{m=-\infty}^{m=\infty} \int_0^k |\mathbf{e}_{\text{TM}}(m,\mathbf{r}_0)\cdot\mathbf{d}|^2 \frac{k}{\nu} dh \right.$$
$$\left. + \sum_{m=-\infty}^{m=\infty} \int_0^k |\mathbf{e}_{\text{TE}}(m,\mathbf{r}_0)\cdot\mathbf{d}|^2 \frac{k}{\nu} dh \right). \tag{A17}$$

Substituting the expressions for photon wave functions, Eqs. (A4) and (A8), into Eq. (A17), and making substitutions (A16), one can obtain the expressions (19)–(21), presented in Sec. II.

In the case when the dipole transitions are forbidden, that is in the case of quadrupole transitions, by the expansion of wave functions in Eq. (A15) we can find the following expression for the decay rate:

$$\gamma_Q = \frac{L\Lambda}{36\pi\hbar^2 c}\left(\sum_{m=-\infty}^{m=\infty} \int_0^k |\nabla_i \mathbf{e}_{\text{TM},j}(m,\mathbf{r}_0)D_{ij}|^2 \frac{k}{\nu} dh \right.$$
$$\left. + \sum_{m=-\infty}^{m=\infty} \int_0^k |\nabla_i \mathbf{e}_{\text{TE},j}(m,\mathbf{r}_0)D_{ij}|^2 \frac{k}{\nu} dh \right). \tag{A18}$$

In Eq. (A17) D_{ij} is the quadrupole momentum tensor,

$$D_{ij} = e\langle(3x_i x_j - x^2\delta_{ij})\rangle_{fi}. \tag{A19}$$

The covariant derivative of the photon electric field in the cylindrical frame of reference is given by:

$$\nabla_k e_i = \frac{1}{H_k}\frac{\partial e_i}{\partial x^k} - \frac{e_k}{H_i H_k}\frac{\partial H_k}{\partial x^i} + \frac{\delta_{ik}}{H_k}\sum_{\lambda=1}^{3}\frac{e_\lambda}{H_\lambda}\frac{\partial H_i}{\partial x^\lambda} \tag{A20}$$

where $H_i = (1,r,1)_i$ are the Lamé coefficients of the cylindrical coordinate system.

Notice that the expression for the decay rate of quadrupole transitions in the absence of a cylinder (free space) has the following form:

$$\gamma_{Q,0} = \frac{k^5}{90\hbar} \sum_{i,j} |D_{ij}|^2. \tag{A21}$$

Substituting the expressions for photon wave functions, Eqs. (A4) and (A8) into Eq. (A18) and making substitutions (A16), one can obtain the expressions for decay rates for quadrupole transitions between arbitrary states.

The simplest expressions are obtained for transitions from the $|l=2, m=0\rangle$ to the $|l=0, m=0\rangle$ state. In this case the tensor of the quadrupole momentum has a diagonal form and with different orientations of the quantization axis we arrive at expressions (41)–(43) from Sec. III.

For transitions with a change of magnetic quantum number, for example, for transitions from $|l=2, m=1\rangle$ to $|l=0, m=0\rangle$, the tensor of quadrupole momentum has the form

$$D_{ij} = D_1 \begin{bmatrix} 0 & 1 & i \\ 1 & 0 & 0 \\ i & 0 & 0 \end{bmatrix}_{ij}. \tag{A22}$$

As a result the expression for the quadrupole decay rate from $|l=2, m=1\rangle$ to $|l=0, m=0\rangle$ in free space has the form

$$\gamma_{Q,0} = \frac{2k^5 |D_1|^2}{45\hbar}. \tag{A23}$$

If the quantization axis is chosen along radius ρ, from Eqs. (A18), (A16), and (A23) we obtain the following expression for the quadrupole decay rate between the $|l=2, m=1\rangle$ and $|l=0, m=0\rangle$ states ($\rho_0 = b$):

$$\frac{\gamma_Q}{\gamma_{Q,0}} = \frac{5}{4} \sum_{m=-\infty}^{\infty} \int_0^k \frac{dh}{k^5} \frac{4h^2 m^2 \nu^2 [(d/dt)\{[J_m(t) - q_{TM} Y_m(t)]/t\}]_{t=\nu b}^2 + (\nu^2 - h^2)^2 [J'_m(t) - q_{TM} Y'_m(t)]_{t=\nu b}^2}{1 + q_{TM}^2}$$

$$+ \frac{5}{4} \sum_{m=-\infty}^{\infty} \int_0^k \frac{dh \, \nu^2}{k^3} \frac{[t(d/dt)\{(J'_m(t) - q_{TE} Y'_m(t))/t\} + (m^2/t^2)\{J_m(t) - q_{TE} Y_m(t)\}]_{t=\nu b}^2}{1 + q_{TE}^2}$$

$$+ \frac{5}{4} \sum_{m=-\infty}^{\infty} \int_0^k \frac{dh}{k^3} \frac{m^2 h^2}{(\nu b)^2} \frac{[J_m(t) - q_{TE} Y_m(t)]_{t=\nu b}^2}{1 + q_{TE}^2}. \tag{A24}$$

On the cylinder surface ($b=a$) we have from Eq. (A24)

$$\frac{\gamma_Q}{\gamma_{Q,0}} = \frac{5}{\pi^2 (ka)^2} \sum_{m=-\infty}^{\infty} \int_0^k dh \frac{4h^2 m^2 \nu^2/(\nu a)^2 + (\nu^2 - h^2)^2}{k^5 |H_m^{(1)}(\nu a)|^2} + \frac{5}{\pi^2 (ka)^2} \sum_{m=-\infty}^{\infty} \int_0^k dh \frac{\nu^2 [2m^2/(\nu a)^2 - 1]^2 + h^2 m^2/(\nu a)^2}{k^3 |(d/dt)[H_m^{(1)}(t)]|_{t=\nu a}^2}. \tag{A25}$$

The decay rates for other transitions have a similar form.

[1]

[1] I. I. Sobelman, *Atomic Spectra and Radiative Transitions* (Springer-Verlag, Berlin, 1979).
[2] S. Haroche, in *Fundamental Systems in Quantum Optics*, Proceeding of the Les Houches Summer School of Theoretical Physics, Session LIII, 1990, edited by J. Dalibard, J.-M. Raimond, and J. Zinn-Justin (North Holland, Amsterdam, 1992), p. 766.
[3] J. M. Wylie and J. E. Sipe, Phys. Rev. A **30**, 1185 (1984); **32**, 2030 (1985).
[4] V. V. Klimov and V. S. Letokhov, Phys. Rev. A **54**, 4408 (1996).
[5] V. V. Klimov and V. S. Letokhov, Comments At. Mol. Phys. (to be published).
[6] J. P. Dowling and J. Gea-Banacloche, Adv. At., Mol., Opt. Phys. **36**, 1 (1996).
[7] S. R. Friberg and R. J. Hawkins, J. Opt. Soc. Am. B **12**, 166 (1995).
[8] J. Denschlag, G. Umshaus, and J. Schmiedmayer, Phys. Rev. Lett. **81**, 737 (1998).
[9] M. Boustimi *et al.* (unpublished); M. Ducloy, in *Nanoscale*

Science and Technology, edited by N. Garcia *et al.* (Kluwer, Dordrecht, 1998), pp. 235–253.
[10] W. S. Lucke, J. Appl. Phys. **22**, 14 (1951).
[11] G. T. Markov and A. F. Chaplin, *Excitation of Electromagnetic Waves* (Radio I Svyaz, Moscow, 1983) (in Russian).
[12] J. J. Bowman, T. B. A. Senior, and P. L. E. Uslenghi, *Electromagnetic and Acoustical Scattering by Simple Shapes* (North-Holland, Amsterdam, 1969).
[13] H. Nha and W. Jhe, Phys. Rev. A **56**, 2213 (1997).
[14] M. A. Rippin and P. L. Knight, J. Mod. Opt. **43**, 807 (1996).
[15] J. D. Jackson, *Classical Electrodynamics* (Wiley, New York, 1975).
[16] J. A. Stratton, *Electromagnetic Theory* (McGraw-Hill, New York, 1941).
[17] J. M. Blatt and V. F. Weisskopf, *Theoretical Nuclear Physics* (Wiley, New York, 1952).
[18] N. E. Kochin, *Calculus of Vectors and Principles of the Calculus of Tensors* (ONTI, Moscow, 1937).
[19] G. N. Watson, Proc. R. Soc. London, Ser. A **95**, 83 (1919–20).
[20] *Handbook of Mathematical Functions*, edited by M.

Abramowitz and I. A. Stegun (Dover, New York, 1964).

[21] C. Dekker, Phys. Today **52** (5), 22 (1999).

[22] R. Saito, G. Dresselhaus, and M. S. Dresselhaus, *Physical Properties of Carbon Nanotubes* (Imperial College Press, London, 1998).

[23] V. V. Klimov, M. Ducloy, and V. S. Letokhov, J. Mod. Opt. **43**, 2251 (1996).

[24] L. de Broglie, *Problèmes de Propagation Guidées des Ondes Electromagnetiques* (Gauthier-Villard, Paris, 1941).

[25] E. Fermi, Rev. Mod. Phys. **4**, 87 (1932).